Virtual-Z Gates and Symmetric Gate Compilation

Arian Vezvaee,[1,2,3,*,†] Vinay Tripathi,[2,4,†] Daria Kowsari,[2,4] Eli Levenson-Falk,[1,2,3,4] and Daniel A. Lidar[1,2,3,4,5,‡]

[1] *Department of Electrical and Computer Engineering, University of Southern California, Los Angeles, California 90089, USA*

[2] *Center for Quantum Information Science & Technology, University of Southern California, Los Angeles, California 90089, USA*

[3] *Quantum Elements, Inc., Thousand Oaks, California 91361, USA*

[4] *Department of Physics and Astronomy, University of Southern California, Los Angeles, California 90089, USA*

[5] *Department of Chemistry, University of Southern California, Los Angeles, California 90089, USA*

(Received 11 August 2024; revised 4 March 2025; accepted 9 May 2025; published 10 June 2025)

The virtual-Z (vz) gate has been established as an important tool for performing quantum gates on various platforms, including but not limited to superconducting systems. Many such platforms offer a limited set of calibrated gates and compile all other gates using combinations of X-type and vz gates. Here, we show that the method of compilation has important consequences in an open quantum system setting. Specifically, we experimentally demonstrate that it is crucial to choose a compilation that is symmetric with respect to vz rotations. An important example is dynamical-decoupling (DD) sequences, where improper gate decomposition can result in unintended effects such as the implementation of the wrong sequence. Our findings indicate that in many cases the performance of DD is adversely affected by the incorrect use of vz gates, compounding other coherent pulse errors. This holds even for DD sequences designed to be robust against systematic control errors. In addition, we identify another source of coherent errors: interference between consecutive pulses that follow each other too closely. This work provides insights into improving general quantum gate performance and optimizing DD sequences in particular.

DOI: 10.1103/PRXQuantum.6.020348

I. INTRODUCTION

Any quantum computing processor is inherently an open quantum system that interacts with its environment, leading to decoherence and errors, which adversely affect quantum computations [1]. Various error-correction, suppression, and mitigation techniques are employed to suppress these effects [2–5]. There has been great interest in demonstrations of overcoming decoherence, which have recently become possible with the availability of commercial cloud-based quantum processors [6–10]. These quantum processors usually have a native set of calibrated gates from which all other gates can be constructed. An important part of the native gate set is the virtual-Z (vz) gate, which is an instantaneous error-free operation that plays a central role in gate compilation. In Ref. [11], the authors have demonstrated that vz gates can be implemented by simply adding a phase offset in software, unlike physical Z gates that involve physical rotations around the z axis of the Bloch sphere. Moreover, they have shown, by manipulating the phases of pulses driving the qubits, that vz gates can be effectively combined with two $\sqrt{X}$ gates to construct any SU(2) gate, thus achieving universality when combined with a two-qubit entangling gate [12,13]. This approach simplifies the gate-decomposition and circuit-compilation procedure, and its applicability extends beyond qubits to qudits as well as beyond superconducting systems [14–20]. Compiling an arbitrary SU(2) operation using vz gates provides flexibility, but ensuring accuracy in the presence of open quantum system effects is essential for reliable computations. Although different compilations involving vz gates can be equivalent in closed systems, discrepancies may arise if open-system effects are not correctly accounted for during compilation.

In this work, we investigate the role of vz gates in gate compilation within an open quantum system dynamics

*Contact author: vezvaee@usc.edu

†These two authors contributed equally to this work.

‡Contact author: lidar@usc.edu

Published by the American Physical Society under the terms of the Creative Commons Attribution 4.0 International license. Further distribution of this work must maintain attribution to the author(s) and the published article's title, journal citation, and DOI.

framework. We find that even slight variations in the compilation of quantum gates using vz gates has significant impact. Specifically, an asymmetric compilation relative to vz gates of any gate corresponding to a rotation about an axis in the x-y plane leads to noticeable effects in various settings, including dynamical decoupling (DD) and algorithm execution. For example, asymmetric compilation of the Y gate introduces fidelity discrepancies between the Y eigenstates $|\pm i\rangle$, which can be completely mitigated with proper compilation techniques. This observation has important consequences, which we explore in this work.

Asymmetric compilation affects the implementation of DD sequences [21–35], potentially leading to misimplementation and misidentification of commonly used sequences. For example, DD implementations using cloud quantum processors reveal unexpected pulse-interval effects, as well as unexplained significant oscillations in single-qubit experiments [34]. In addition, our findings uncover previously unrecognized oscillations, even in DD sequences designed to be robust to coherent errors [30–32]. The investigations into the vz gate that we report here reveal that interference between consecutive pulses explains these oscillations in robust sequences. Given the recent critical role that DD has played in improving the fidelity of quantum states [33,34,36–40], circuits [41–43], and even entire algorithms [44–47], we expect these findings to contribute to further improvement of quantum error suppression via pulse-based methods such as DD. However, the impact extends beyond DD to any quantum algorithm or error-correction method that requires high-fidelity single-qubit gates.

The structure of this paper is as follows. In Sec. II, we provide the theoretical background to the difference between symmetric and asymmetric gate compilation in an open-system setting. This includes a discussion of coherent error sources, an intuitive trajectory-based picture for symmetric versus asymmetric compilation, and the impact on DD. Section III contains all our experimental results, obtained using our in-house MUNINN processor as well as IBMQ devices. We present results for various DD sequences and Greenberger-Horne-Zeilinger (GHZ) state fidelity, and analyze pulse-interference effects. Our results present strong confirmation of the advantage offered by symmetric gate compilation. We conclude in Sec. IV.

II. vz GATE IN AN OPEN QUANTUM SYSTEM

We conduct all our experiments using two superconducting transmon quantum processors: the IBM cloud quantum processor IBM_SHERBROOKE and our in-house quantum processor MUNINN [48]; the design can be found in the SQuADDS database [49].

We model the transmon qubit as a driven two-level system and consider it in the drive frame under the rotating-wave approximation (e.g., Ref. [50]). Let $\{\sigma_\alpha\}$ denote the set of Pauli matrices. The time-dependent system Hamiltonian that generates single-qubit X-rotation gates is given by

$$H(t) = \varepsilon_{\rm tot}(t)\frac{\sigma_x}{2} + H_{\rm err}, \tag{1a}$$

$$H_{\rm err} = \varepsilon_{\rm err}\frac{\sigma_x}{2} + \Delta_{\rm err}\frac{\sigma_z}{2}. \tag{1b}$$

Here, $\varepsilon_{\rm tot}(t)$ is the intended time-dependent control field and $\varepsilon_{\rm err}$ and $\Delta_{\rm err}$ are errors. Ideally, $\varepsilon_{\rm err} = \Delta_{\rm err} = 0$. In reality, both are present and give rise to rotation and phase errors

$$\delta\theta \equiv \varepsilon_{\rm err} t_g, \quad \delta\varphi \equiv \frac{\Delta_{\rm err}}{\bar{\varepsilon}} = \frac{1}{\theta}\Delta_{\rm err} t_g, \tag{2}$$

respectively, with t_g denoting the gate duration, $\theta \equiv \int_0^{t_g} \varepsilon_{\rm tot}(t)\,dt$, and $\bar{\varepsilon} = \theta/t_g$ as the average pulse amplitude [51]. An open-system single-qubit gate includes both rotation and phase errors, as well as a system-bath interaction term that is always present while the gate is being generated.

A. Gate compilation

vz gates eliminate the need for performing physical rotations about the Bloch z axis, allowing us to focus solely on rotations in the x-y plane. We denote by $R_\phi(\theta)$ a rotation by an angle θ about an arbitrary axis in the x-y plane, making an angle ϕ with the x axis:

$$R_\phi(\theta) \equiv \exp\left[-i(\theta/2)(\cos(\phi)\sigma_x + \sin(\phi)\sigma_y)\right]. \tag{3}$$

We also denote

$$R_x(\theta) \equiv R_{\phi=0}(\theta), \quad R_y(\theta) \equiv R_{\phi=\pi/2}(\theta). \tag{4}$$

The physical implementation of $R_\phi(\theta)$ involves applying an on-resonance microwave pulse of the form $\varepsilon_{\rm tot}(t) = \varepsilon(t)\cos(\omega t + \phi)$ to the qubit, where the integrated pulse amplitude (for a given pulse duration) determines θ and the pulse phase determines ϕ. The phase ϕ is arbitrary, as is the choice of the x-y coordinate system, both set by the initial pulse. This illustrates how the vz gate is implemented simply by updating the definition of which pulse phase corresponds to $\phi = 0$ (usually set to be the x axis, as above). However, this adjustment has tangible physical effects on subsequent gates: after a virtual $R_z(\varphi) \equiv \exp[-i(\varphi/2)\sigma_z]$ gate [note that $R_z(\pi) \equiv Z = -i\sigma_z$], the phase of each of the rotations that follow is shifted by φ. For example, when $\varphi = \pi$, then the next operation $R_x(\theta)$ becomes $R_\pi(\theta) = R_{-x}(\theta)$, i.e., a rotation about the x axis becomes a rotation about the $-x$ axis, in the sense that $R_{-x}(\theta) = R_z^\dagger(\pi)R_x(\theta)R_z(\pi)$.

For most commercial cloud-based quantum processors, not all rotations are natively available. For example, for the

IBMQ devices, the calibrated single-qubit native gate set typically consists of the operations $\mathcal{G} = \{R_z(\varphi), \sqrt{X}, X\}$, where $\sqrt{X} \equiv R_x(\pi/2)$ and $X \equiv R_x(\pi) = -i\sigma_x$, which are generated using $H(t)$ given in Eq. (1). However, these are not the only Clifford operations necessary for universal quantum computation. All other Clifford gates must be decomposed into these operations. Specifically, a $Y \equiv R_y(\pi) = -i\sigma_y$ gate requires an X gate combined with vz gates, which can be done in different ways. One method of compiling a Y gate is asymmetric:

$$Y^{\text{asym}} = XR_z(-\pi). \tag{5}$$

Alternatively, a symmetric compilation of the Y gate with respect to the vz gates is

$$Y^{\text{sym}} = R_z(\pi/2)XR_z(-\pi/2). \tag{6}$$

Although these methods are theoretically equivalent in the sense that $Y^{\text{asym}} = Y^{\text{sym}} = Y$ is a mathematical identity, this is no longer the case when one accounts for deviations from unitary dynamics due to open quantum system effects, as we discuss in detail below.

B. Trajectories matter: Asymmetry between $|+i\rangle$ and $|-i\rangle$

To demonstrate how the two compilation strategies result in different outcomes, we consider a simple experiment, in which we apply sequences with a varying number of YY pulses to the two orthogonal initial states $|\pm i\rangle$. Ideally, the fidelity of YY applied to $|+i\rangle$ or $|-i\rangle$ should be identical. However, with the asymmetric decomposition, the two states follow different Bloch-sphere trajectories and leave the x-y plane. That is, in the case of Y^{asym}, the virtual $R_z(-\pi)$ gate instantaneously interchanges $|+i\rangle$ and $|-i\rangle$ (up to a global phase of i) before the physical X gate is applied. This has the effect of $|-i\rangle$ following a trajectory through the stable ground state $|0\rangle$ during the X gate, while $|+i\rangle$ passes through the unstable excited state $|1\rangle$ [see Fig. 1(a)]. The second Y gate leads to a reversal of this trajectory, again passing through the ground or excited state, as the virtual $R_z(-\pi)$ reverses the direction of rotation. Consequently, $|-i\rangle$ experiences a lower relaxation rate and maintains a higher fidelity compared to $|+i\rangle$ over the course of repeated applications of the YY sequence.

Conversely, using the symmetric decomposition Y^{sym}, the first vz gate, $R_z(-\pi/2)$, transforms $|-i\rangle$ to $|-\rangle$ and $|+i\rangle$ to $|+\rangle$ (up to a global phase of $e^{i\pi/4}$). These states then undergo an X gate, which leaves them unchanged (up to a global phase). The next vz gate, $R_z(\pi/2)$, transforms the state back to its original position on the y axis. Therefore, with this compilation, $|\pm i\rangle$ both remain in the x-y plane at all times during the Y^{sym} gate and do not experience different relaxation rates. As a result, the fidelities of $|\pm i\rangle$ should be similar under YY, as for a physical Y gate. By linearity, this extends to any state in the x-y plane, i.e., to any superposition of $|\pm i\rangle$ or $|\pm\rangle$. Another way to see this result is that symmetric YY compiles to two repetitions of Eq. (6), which is then equal to $R_z(\pi/2)XXR_z(-\pi/2)$. The interior XX sequence traces out a full 2π rotation and thus always leads to trajectories that trace the same paths for any two opposite initial states, as expected by the YY sequence.

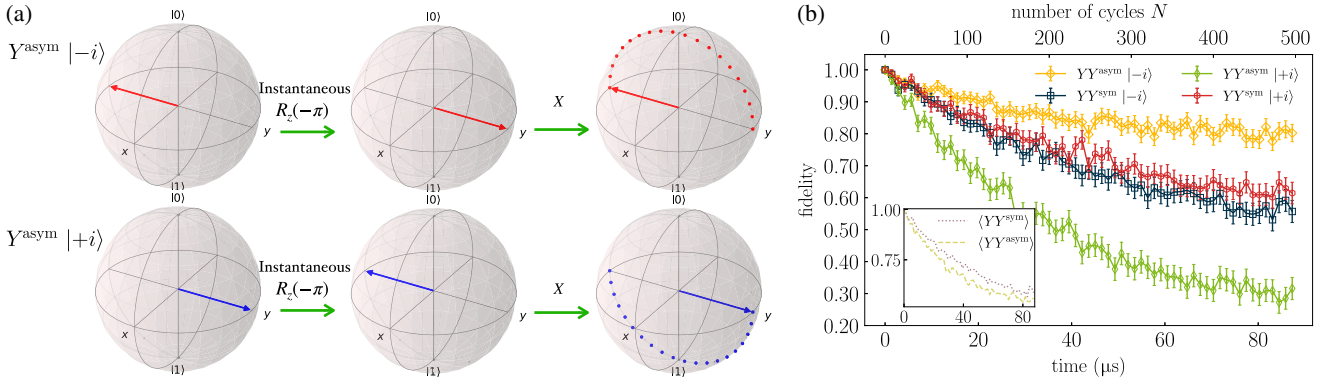

FIG. 1. The open-system effect of the symmetric and asymmetric compilation of the Y gate with respect to vz gates. (a) The $|\pm i\rangle$ state follows different Bloch-sphere trajectories under Y^{asym}, which consist of an instantaneous vz gate followed by a physical X gate. This causes $|-i\rangle$ ($|+i\rangle$) to go through a stable (unstable) ground (excited) state that leads to the asymmetry in the fidelity of the two states. The symmetric decomposition Y^{sym} overcomes this asymmetry, similar to a physical Y gate. (b) An experimental demonstration of the symmetric and asymmetric effects of the Y-gate decomposition on the MUNINN processor. The fidelity of the states $|\pm i\rangle$ is shown under both Y^{asym} and Y^{sym}, as a function of time (bottom axis) or number of YY sequence cycles (top axis). The symmetric decomposition results in similar fidelities (black and red) for the initial states $|\pm i\rangle$. The asymmetric decomposition results in very different fidelities (yellow and green) for the same two initial states, in agreement with our theoretical prediction of a higher fidelity for the $|-i\rangle$ state, the trajectory of which passes through the ground state $|0\rangle$. The inset shows the average fidelity of the two input states in each case. Here and in all other figures, the error bars denote two standard deviations of the mean.

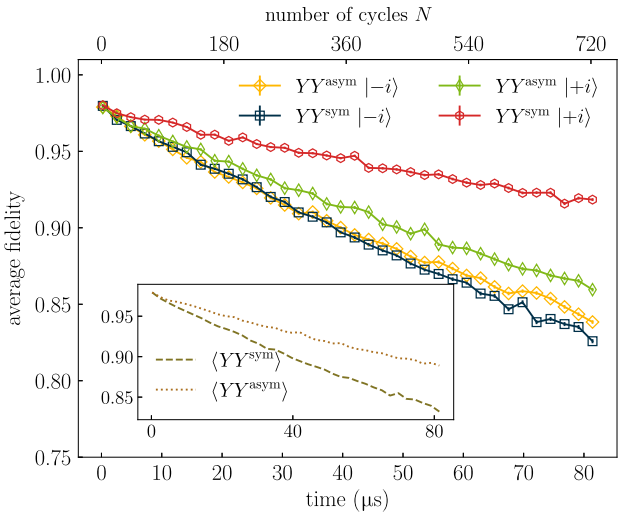

FIG. 2. The effect of the asymmetric Y^{asym} and symmetric Y^{sym} gates on the state fidelity averaged over four qubits (0, 13, 81, 89) of the IBM_SHERBROOKE processor. The fidelity is shown as a function of time (bottom) or the number of cycles of the YY sequence (top). Subject to Y^{sym}, the fidelities of the $|\pm i\rangle$ states (black and red) are significantly closer than those subject to Y^{asym} (yellow and green). The inset shows the average fidelity of the two input states in each case.

We have verified the effects predicted above through various experiments, using both the IBM_SHERBROOKE and MUNINN processors. As described above, we first prepare the initial states $|\pm i\rangle$, apply a series of YY sequences, unprepare the initial state, and measure the system in the σ_z eigenbasis. We define the empirical fidelity as the frequency of favorable outcomes, i.e., the number of $|0\rangle$ outcomes divided by the total number of experimental shots (800). In Fig. 1(b), we show the results for the MUNINN processor. A correctly implemented Y gate does not discriminate between the states $|+i\rangle$ and $|-i\rangle$ except for a global phase, i.e., it yields the same fidelity on both states. The same must hold for a well-calibrated physical Y gate and this is what Fig. 1(b) shows for the symmetric compilation. The fact that the asymmetric compilation results in the predicted fidelity asymmetry between the $|\pm i\rangle$ states is a clear demonstration of the problematic nature of this compilation. We observe the same effect after repeating the experiments on different qubits of the IBM_SHERBROOKE processor, as highlighted in Fig. 2.

We note that the importance of the results shown in Fig. 1(b) is not that the symmetric compilation achieves a higher fidelity (insets of Figs. 1 and 2) but, instead, that only symmetric compilation results in the correct fidelity behavior that does not distinguish between $|+i\rangle$ and $|-i\rangle$.

C. Impact on DD sequences

Next, we consider the impact of symmetric versus asymmetric compilation on DD sequences.

1. Correct $\overline{X} \equiv R_x(-\pi)$

As discussed earlier, the vz gates enact a frame transformation for all subsequent gates. In the present context, this manifests as the identity

$$R_x(\pi)R_z(\pm\pi) = -R_z(\mp\pi)R_x(-\pi). \tag{7}$$

The frame transformation defined by Eq. (7) can be reinterpreted as a way to create a correct $\overline{X} \equiv R_x(-\pi)$ gate, which plays an important role in robust DD sequences [31,32,52]. Namely, we perform the symmetric version of the gate as

$$\overline{X} = R_z(-\pi)XR_z(\pi) \quad \text{or} \quad R_z(\pi)XR_z(-\pi). \tag{8}$$

As we show in Sec. III, performing the correct $\overline{X}$ gate is critical for understanding the oscillations in the fidelity of the robust DD sequences that have been observed on IBM devices [34]. In particular, it is essential that the implemented physical rotation is $R_x(-\pi)$ as opposed to $R_x(\pi)$ along with subsequent frame updates.

2. Symmetric Y yields XY4

One of the fundamental DD sequences is XY4 [53]:

$$\text{XY4} \equiv Yf_\tau Xf_\tau Yf_\tau Xf_\tau, \tag{9}$$

where $f_\tau = e^{-i\tau H}$ denotes the free-evolution unitary generated by the total system-bath Hamiltonian H and τ is the pulse interval, i.e., the delay between two consecutive pulses. XY4 is also known as the universal decoupling sequence, as it decouples arbitrary single-qubit decoherence [22].

We now demonstrate that symmetric compilation yields XY4. Toward this end, first note the identity

$$R_x(\pi)R_z(-\pi/2) = R_z(-\pi/2)R_y(\pi), \tag{10}$$

i.e., $R_z(-\pi/2)$ changes the rotation axis of the subsequent gates by $\pi/2$, transforming $R_x(\pi) \to R_y(\pi)$. Therefore, using Y^{sym} [Eq. (6)], we have

$$\begin{aligned}
\text{XY4}^{\text{sym}} &= R_z(\pi/2)R_x(\pi)R_z(-\pi/2)f_\tau R_x(\pi)f_\tau \\
&\quad \times R_z(\pi/2)R_x(\pi)R_z(-\pi/2)f_\tau R_x(\pi)f_\tau \\
&= R_z(\pi/2)R_z(-\pi/2)R_y(\pi)f_\tau R_x(\pi)f_\tau \\
&\quad \times R_z(\pi/2)R_z(-\pi/2)R_y(\pi)f_\tau R_x(\pi)f_\tau \\
&= R_y(\pi)f_\tau R_x(\pi)f_\tau R_y(\pi)f_\tau R_x(\pi)f_\tau,
\end{aligned} \tag{11}$$

which is indeed the XY4 sequence given in Eq. (9).

3. Asymmetric Y yields $\mathbf{UR_4}$ *instead of XY4*

Using the asymmetric definition of the Y gate [Eq. (5)], the XY4 sequence becomes

$$\begin{aligned}&\mathrm{XY4}^{\mathrm{asym}}\\&\quad= R_x(\pi)R_z(-\pi)f_\tau R_x(\pi)f_\tau R_x(\pi)R_z(-\pi)f_\tau R_x(\pi)f_\tau.\end{aligned} \tag{12}$$

Using Eq. (7) allows us to commute the vz gate to the left. Since it is a virtual gate implemented via phase offsets in software, the vz gate commutes with the free-evolution operator f_τ. Dropping overall phase factors, we can thus rewrite $\mathrm{XY4}^{\mathrm{asym}}$ as follows:

$$\begin{aligned}&\mathrm{XY4}^{\mathrm{asym}}\\&\quad= R_x(\pi)R_z(-\pi)f_\tau R_x(\pi)R_z(\pi)f_\tau R_x(-\pi)f_\tau R_x(\pi)f_\tau\\&\quad= R_x(\pi)R_z(-2\pi)f_\tau R_x(-\pi)f_\tau R_x(-\pi)f_\tau R_x(\pi)f_\tau\\&\quad= R_x(\pi)f_\tau R_x(-\pi)f_\tau R_x(-\pi)f_\tau R_x(\pi)f_\tau.\end{aligned} \tag{13}$$

In fact, this sequence is the fourth-order "universally robust" sequence [32]

$$\mathrm{UR}_4 = Xf_\tau\overline{X}f_\tau\overline{X}f_\tau Xf_\tau, \tag{14}$$

rather than the intended XY4; i.e.,

$$\mathrm{XY4}^{\mathrm{asym}} = \mathrm{UR}_4. \tag{15}$$

4. Generalization to $\mathbf{UR}_n$

UR_4 is the lowest-order sequence in the UR_n family, defined as

$$\mathrm{UR}_n = R_{\phi_n}(\pi)f_\tau\cdots R_{\phi_2}(\pi)f_\tau R_{\phi_1}(\pi)f_\tau, \tag{16a}$$

$$\phi_k = \frac{(k-1)(k-2)}{2}\Phi^{(n)} + (k-1)\phi_2, \tag{16b}$$

$$\Phi^{(4m)} = \frac{\pi}{m}\Phi^{(4m+2)} = \frac{2m\pi}{2m+1}, \tag{16c}$$

where $R_\phi(\pi)$ is a π rotation about an axis that makes an angle ϕ with the x axis, as defined in Eq. (3). The phase ϕ_1 is set to zero without loss of generality. The phase ϕ_2 can be chosen at will and when it is set to $\pi/2$ for $n = 4$ one recovers the XY4 sequence, i.e., $\mathrm{XY4}^{\mathrm{sym}}$. Following Ref. [32], we set $\phi_2 = \pi$, yielding UR_4.

Theory predicts that the UR_n family of sequences is robust against systematic rotation and phase errors [Eq. (2)], i.e., an infidelity that decreases exponentially in the sequence order n at a cost that grows only linearly in n [32]. In this sense, the fact that asymmetric compilation yields UR_4 rather than XY4 can be viewed as an advantage if the goal is only to suppress dephasing. However, unlike the universal XY4 sequence, UR_4 cannot suppress multiaxis errors. From this perspective, asymmetric compilation has resulted in a loss of multiaxis suppression capabilities. Note also that since XY4 is a member of the UR_n family (as noted above), it is expected to exhibit the same robustness properties as UR_4.

Nevertheless, since it amounts to a type of inherent fault tolerance, there is significant interest in demonstrating the improvement in systematic error suppression associated with the UR_n family. This requires a correct implementation of $R_\phi(\pi)$, i.e., a rotation about an arbitrary axis in the x-y plane.

While in principle one can write the required arbitrary axis rotations as

$$R_\phi^{\mathrm{asym}}(\pi) \equiv XR_z(-2\phi), \tag{17}$$

only the symmetric choice yields the correct universally robust sequence:

$$R_\phi^{\mathrm{sym}}(\pi) \equiv R_z(-\phi)XR_z(\phi). \tag{18}$$

This is the most general form of a π rotation about an arbitrary axis in the x-y plane. In fact, Eqs. (6) and (8) are the special cases of $\phi = \pi/2$ and $\phi = \pi$, respectively. We demonstrate the performance impact on UR_n of the symmetric and asymmetric versions of $R_\phi(\pi)$ in Secs. III A and III B.

D. Quantum circuits using symmetric versus asymmetric compilation

As we have just seen, the choice between symmetric or asymmetric compilation is not limited to Y or $\overline{X}$ gates but applies to any axis of rotation in the x-y plane. This has significant implications beyond DD and is relevant to a broad range of quantum algorithms. We demonstrate the effect of symmetric versus asymmetric compilation on different types of quantum circuits in the Appendix. These demonstrations contrast circuits employing symmetric compilation [Eq. (18)] instead of its asymmetric counterpart [Eq. (17)].

III. EXPERIMENTAL VERIFICATION

In this section, we report on various experiments to test our predictions about the role of vz gates in open quantum systems. We present both DD experiments and quantum circuits corresponding to GHZ-state preparation. The results illustrate the importance of the choice of symmetric compilation in the implementation of quantum circuits.

A. DD sequence implementation using symmetric versus asymmetric compilation

To test our prediction that when using Y^{asym}, XY4 is effectively the same as UR_4, in Fig. 3(a) we present the results of measuring the fidelity of the $|+\rangle$ state as a function of time for a variety of different pulse

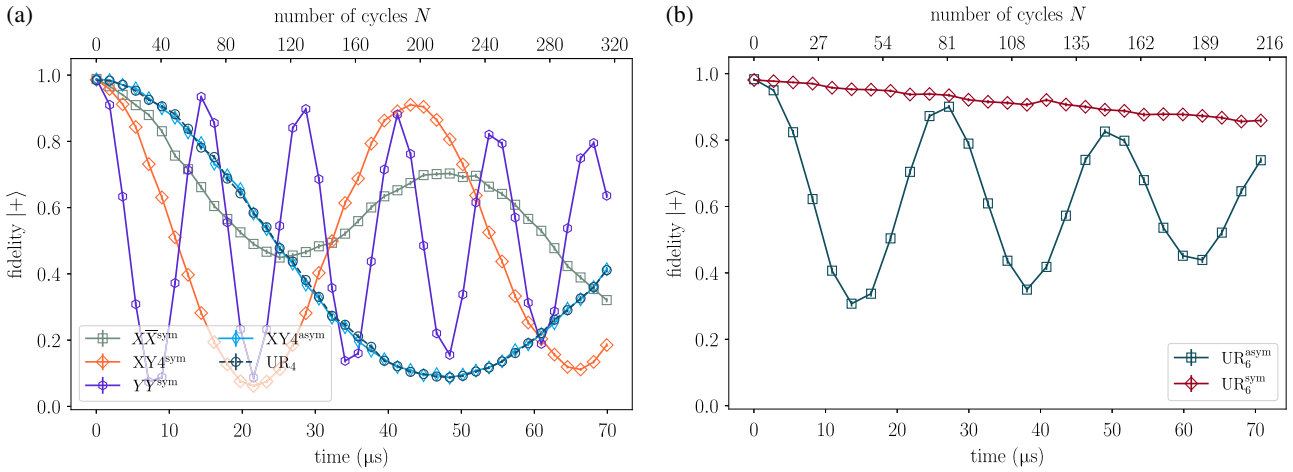

FIG. 3. (a) The $|+\rangle$ state fidelity as a function of total sequence time (or number of sequence cycles; top axis), subject to the $XY4^{\text{sym}}$, $XY4^{\text{asym}}$, UR_4, YY^{sym}, and $X\overline{X}$ sequences applied to a single qubit (qubit 37) on the IBM_SHERBROOKE device. Data points for the two-pulse-long YY^{sym} and $X\overline{X}$ sequences are shown for every second cycle (i.e., their total number of cycles is 640). The $XY4^{\text{asym}}$ and UR_4 sequences exhibit nearly identical fidelity decay behavior, clearly distinct from that of the $XY4^{\text{sym}}$ sequence, confirming that the asymmetric Y gates transform XY4 into the UR_4 sequence. All sequences shown exhibit oscillations. (b) The $|+\rangle$ state fidelity as a function of total sequence time (or number of sequence cycles; top axis), subject to UR_6^{sym} and UR_6^{asym} applied to qubit 89 on the IBM_SHERBROOKE device. The cycles corresponds to six-pulse sequences. UR_6^{sym} drastically outperforms UR_6^{asym}.

sequences, each of which is applied repeatedly. Specifically, we apply the following sequences to a single qubit on IBM_SHERBROOKE: UR_4 using the symmetric definition for $\overline{X}$ given in Eq. (8), and two versions of XY4 using the symmetric and asymmetric Y gates. As shown in Fig. 3(a), the UR_4 and $XY4^{\text{asym}}$ sequences are almost indistinguishable, as expected. In contrast, $XY4^{\text{sym}}$ is distinct.

It is important to note that QISKIT [54] natively compiles the Y gate in the asymmetric form of Eq. (5). Therefore, caution is necessary when interpreting previously reported DD results involving transmon qubits that did not use the Y^{sym} gate, including numerous studies involving the XY4 sequence.

In Fig. 3(b), we show the performance of the UR_6 sequence: $Xf_\tau R_{2\pi/3}(\pi)f_\tau Xf_\tau Xf_\tau R_{2\pi/3}(\pi)f_\tau Xf_\tau$. For $R_{2\pi/3}(\pi)$, we have used the asymmetric and symmetric decompositions given in Eqs. (17) and (18) in the sequences UR_6^{asym} and UR_6^{sym}, respectively. Evidently, the compilation choice leads to two different sequences, with the symmetric choice significantly outperforming the asymmetric one. In theory, the UR_6 sequence should be robust against coherent errors and exhibit no oscillations. This is indeed what we observe for the symmetric compilation choice. However, the asymmetric choice exhibits strong oscillations, which is a clear indication that the implemented sequence is not universally robust. Thus, the use of symmetric compilation is important not only for Y or $\overline{X}$ gates but also for rotations about arbitrary axes in the x-y plane. The asymmetric choice leads to the wrong implementation of the desired pulse sequence, while the symmetric choice yields the correct sequence.

B. Impact of symmetrically versus asymmetrically compiled gates on GHZ-state fidelity

To test the impact of the choice of compilation beyond the single-qubit case, we now consider the problem of fidelity preservation of GHZ states.

We prepare the three-qubit GHZ state (GHZ_3) and then simultaneously apply even numbers of $R_\phi(\pi)$ rotations with $\phi \in \{\pi/4, \pi/3\}$ to all qubits, implemented according to Eqs. (17) and (18). Note that GHZ-state preparation itself does not involve gates affected by symmetric versus asymmetric compilation. We then unprepare the GHZ_3 state and define the fidelity as retrieving the $|000\rangle$ state. In Fig. 4, we show that this leads to a clear fidelity difference, with symmetric compilation outperforming asymmetric compilation.

As another test, we prepare the GHZ_3 state, apply a certain number of repetitions of UR_n simultaneously to all three qubits for different values of n, unprepare the GHZ_3 state, and measure each qubit in the computational basis. We note that pulse staggering is the better choice for crosstalk suppression [55–57], but for our purposes the simultaneous sequence suffices.

Each UR_n sequence consists of n pulses and we consider $n \in \{4, 8, 16, 32, 64, 128\}$. When we repeat a given UR_n sequence m times ("periodic DD" [58]), the total number of pulses is $p = mn$. We use both the symmetric and asymmetric compilations for each UR_n sequence.

The results in Fig. 5 illustrate that symmetric compilation always yields improved performance. This effect is more significant for smaller n and for larger total pulse number p.

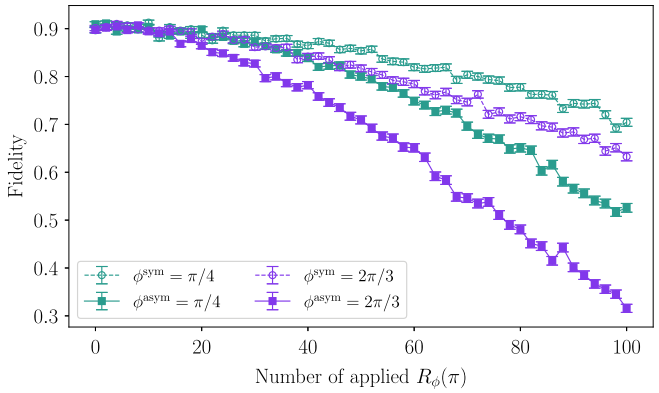

FIG. 4. The impact of symmetric versus asymmetric compilation on rotations in the x-y plane. A GHZ_3 state is prepared and even numbers of symmetric or asymmetric rotations making an angle of $\phi = \pi/4$ or $\phi = 2\pi/3$ with the x axis are applied. The state is then unprepared and the fidelity is measured. The results show that the symmetric compilation consistently achieves higher fidelities compared to the asymmetric approach.

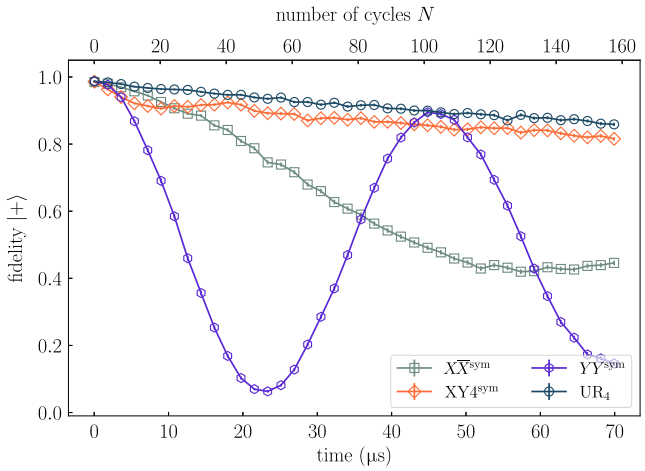

FIG. 6. As in Fig. 3(a) (except for the absence of XY4$^{\rm asym}$) with the pulse interval doubled from $\tau = 56.8$ ns to $2\tau = 113.6$ ns. The oscillation periods of $YY^{\rm sym}$ and $X\overline{X}$ increase significantly and the difference between the now decaying XY4$^{\rm sym}$ and UR$_4$ fidelities is nearly eliminated.

In Fig. 5(b), we also present the first experimental evidence for the theoretically expected improvement with n at constant total pulse number [32]. However, we find that the improvement is observable only for sufficiently long pulse sequences, i.e., $p \geq 64$. Interestingly, the improvement is significantly more pronounced for the asymmetric compilation. A potential explanation is that for low n, the asymmetric sequence deviates more from ideal UR$_n$ than the symmetric sequence and the difference between the two becomes less pronounced with increasing n. For the symmetric compilation, we find that increasing n has only a small effect, except from UR$_4$ to UR$_8$ when $p \geq 64$.

C. Pulse interference

In Fig. 3(a), we also display the YY and $X\overline{X}$ sequences, constructed using the symmetric definitions given in Eqs. (6) and (8), respectively. An unexpected feature observed in Fig. 3(a) is that all five sequences shown (including the robust ones) exhibit oscillations, which

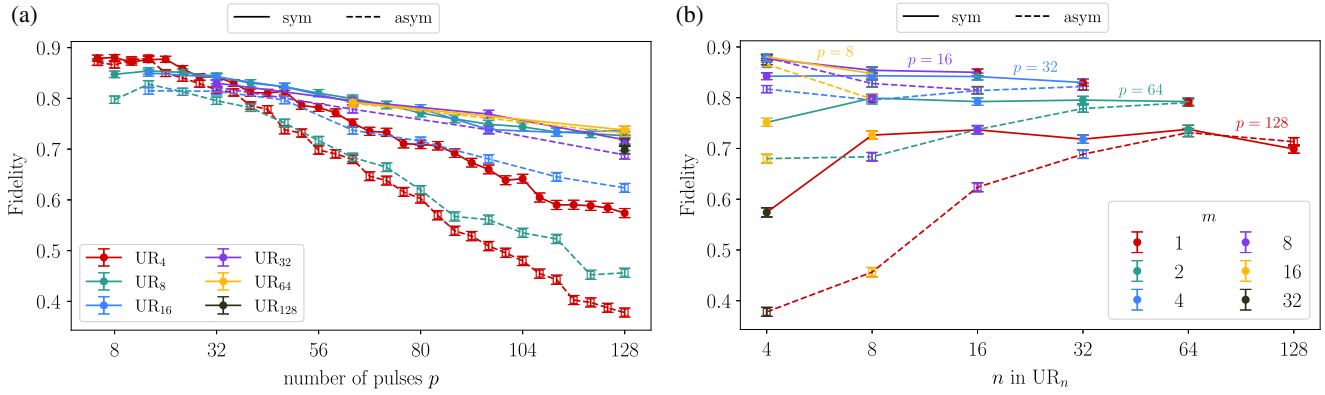

FIG. 5. The fidelity of a three-qubit GHZ state subject to UR$_n$ sequences applied simultaneously to each qubit, using both symmetric and asymmetric compilations. (a) The results as a function of the total number of pulses p (the total time elapsed is $p\tau$, where $\tau = 56.8$ ns). All UR$_n$ sequences are periodically repeated (e.g., UR$_4$ is repeated up to 32 times), with the exception of UR$_{128}$, which is implemented only once. For $n \leq 32$, we observe that symmetric compilation outperforms asymmetric compilation at all times. For $n = 64$ and 128, the two compilations are statistically indistinguishable. (b) A plot of (a subset of) the same data as a function of n for different numbers of sequence repetitions m. Fixing n and reading the results from top to bottom is equivalent to reading (a) from left to right. Reading the results from left to right along the drawn connecting lines gives the performance of UR$_n$ as a function of n at fixed p (total number of pulses). Either way, symmetric compilation outperforms asymmetric compilation. The results at constant p also show that the performance of UR$_n$ deteriorates as a function of n for the shorter sequences ($p \in \{8, 16, 32\}$), and improves with n for the longer sequences ($p \in \{64, 128\}$).

typically arise from coherent errors. We hypothesize that this phenomenon is due to an interference effect between consecutive pulses, e.g., due to an impedance mismatch in the microwave control lines [59]. This causes large enough errors to overwhelm the first-order robustness of UR_4.

To test this hypothesis, we have repeated the same experiments as shown in Fig. 3(a) (except that we have not repeated $XY4^{asym}$, since we have already established its equivalence with UR_4) but with an intentional delay added between consecutive pulses, thus doubling the pulse interval $\tau = 56.8\,\text{ns}$, defined as the time delay between the peaks of two consecutive pulses. The result, shown in Fig. 6, is that the $XY4^{sym}$ and UR_4 sequences no longer oscillate but exhibit simple decay. Moreover, the

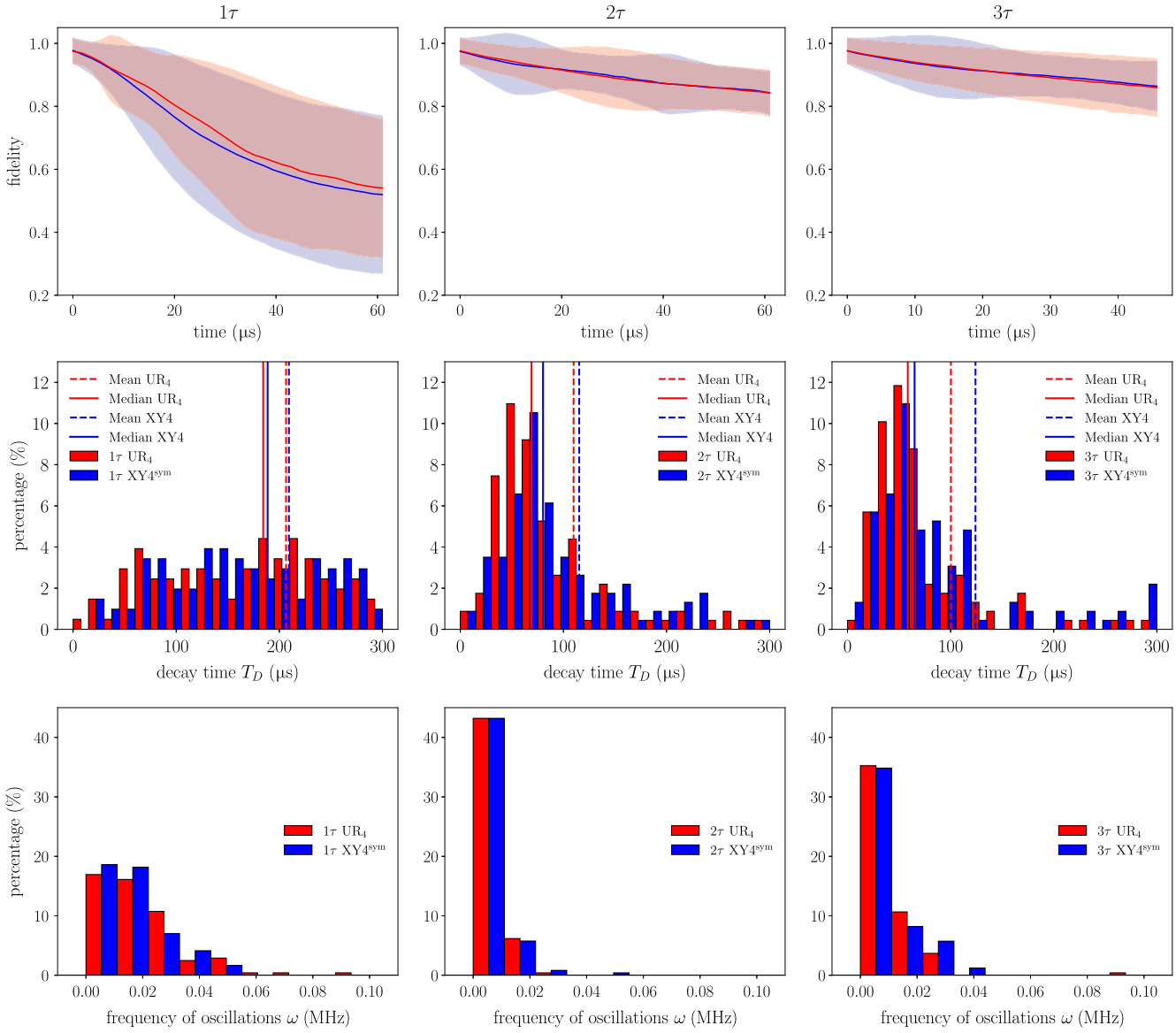

FIG. 7. The fidelities of the $XY4^{sym}$ (blue) and UR_4 (red) sequences with different pulse intervals: $1\tau, 2\tau$, and 3τ (where $\tau = 56.8\,\text{ns}$) for IBM_SHERBROOKE. Top row: the corresponding fidelity means and standard deviations for 123 out of the 127 qubits for the indicated pulse intervals. For 1τ, the UR_4 sequence has a somewhat smaller decay rate. The decay rates decrease significantly at 2τ and 3τ, as do their standard deviations. Middle row: the distribution of fitted decay times T_D from fitting each of the 123 decay curves to $a + be^{-t/T_D}\cos(\omega t)$. The distribution is relatively broad at 1τ and narrows significantly at 2τ and 3τ. Both the mean and median XY4 decay times are slightly larger than those for UR_4 for all pulse intervals, opposite from the top-row result at 1τ. However, note that top row displays the mean at each time, which is different from the mean of the fits shown in the histograms. Bottom row: the distribution of frequency of oscillations. The oscillations are relatively significant at 1τ but as we increase the pulse interval to 2τ and 3τ, the distributions peak around zero, indicating that oscillations are strongly suppressed. The difference in oscillation frequencies between the XY4 and UR_4 sequences is negligible.

stark difference between the latter two sequences seen in Fig. 3(a) has now almost disappeared. This is consistent with the observation that Z (dephasing) errors and rapid (i.e., fast compared to the gate time) relaxation errors are the dominant error source in transmon qubits, so that sequences suppressing X or Y errors have little added benefit over sequences suppressing only Z errors.

The fact that the fidelities seen in Fig. 3(a) are higher for intervals of 2τ rather than τ also helps to explain why previous studies involving transmon qubits [33,34] have observed that, in contrast to the DD theory for ideal zero-width pulses (see, e.g., Ref. [60]), the optimal pulse interval is not always the shortest possible (the same phenomenon has also been observed in other platforms; e.g., nuclear magnetic resonance [61] and trapped ions [62]). The pulse-interference effect, with pulses applied consecutively with the minimum shortest possible pulse interval τ, can introduce additional coherent errors that result in inferior DD performance even with sequences (such as UR_4) that are robust against small coherent errors. Our results confirm the conclusion of Ref. [34] that it is essential to optimize the pulse interval for a given quantum processor, with the added insight that this optimization can reduce or (depending on the pulse sequence) even eliminate coherent errors due to pulse interference.

The reason why we include the $X\overline{X}$ and YY sequences in Fig. 3(a) is that $X\overline{X}$ is susceptible to phase errors, while YY is susceptible to rotation errors [Eq. (2)], as discussed in detail in Ref. [51]. More specifically, Figs. 3 and 6 show that the two sequences exhibit oscillations for both the τ and 2τ cases, with a period significantly shorter than that of the other sequences shown. This is consistent with the existence of single-pulse phase and rotation errors in addition to pulse-interference errors. Doubling the pulse interval significantly increases the oscillation period, as seen in Fig. 6, but does not eliminate the oscillations. Moreover, we have checked (not shown) that further increasing the pulse interval to 3τ has little effect on the $X\overline{X}$ and YY fidelities, showing that coherent phase and rotation errors cannot be eliminated by controlling the pulse-interference effect alone.

In Fig. 6, we display results from a single qubit; to test whether the result of increasing the pulse interval is a statistically significant feature, we have applied the $\mathrm{XY4}^{\mathrm{sym}}$ and UR_4 sequences to all 127 qubits of the IBM_SHERBROOKE device, for pulse intervals of $\tau = 56.8\,\mathrm{ns}$, 2τ, and 3τ. The results are shown in Fig. 7, after removing four of the qubits the measurements for which were inadvertently performed during a calibration cycle (qubits 20, 21, 56, 63).

As seen in the top row, the oscillations exhibited by both $\mathrm{XY4}^{\mathrm{sym}}$ and UR_4 in the 1τ case are significantly reduced for pulse intervals of 2τ and 3τ. The time-averaged decay rate improves significantly when the pulse interval increases from τ to 2τ, showing that an optimized pulse interval (as opposed to the minimum interval) is preferable, consistent with the findings of Ref. [34].

In the middle row of Fig. 7, we plot the distribution of decay times T_D obtained by fitting the fidelities of the $\mathrm{XY4}^{\mathrm{sym}}$ and UR_4 sequences to $a + be^{-t/T_D}\cos(\omega t)$. The distribution is quite broad for both XY4 and UR_4 at 1τ and narrows considerably at 2τ and 3τ, while shifting to the left and peaking at a slightly lower T_D value for UR_4.

Finally, in the bottom row of Fig. 7, we plot the distribution of the frequency of oscillations ω obtained by fitting the fidelities of the $\mathrm{XY4}^{\mathrm{sym}}$ and UR_4 sequences to the same function $a + be^{-t/T_D}\cos(\omega t)$. Evidently, as we increase the pulse interval from τ to 2τ, the distribution moves toward smaller values but broadens again from 2τ to 3τ, suggesting that a 2τ pulse interval is preferred.

Overall, we may conclude that the pulse-interference effect is significant when pulses are applied back to back but is strongly suppressed by increasing the pulse interval. Optimizing the pulse interval can significantly increase the decay time while narrowing its distribution and at the same time drastically reduce fidelity oscillations.

We note that pulse-interference effects have been previously observed (see, e.g., Ref. [35]). The key finding that we report here is the ability to distinguish pulse interference from coherent pulse errors (such as phase and rotation errors) that robust sequences, such as $\mathrm{XY4}^{\mathrm{sym}}$ and UR_4, are designed to withstand. This distinction becomes apparent only after using the correct vz decomposition, as this allows us to implement the intended set of UR_n sequences that are immune to specific coherent errors but not to pulse interference.

IV. CONCLUSIONS

This work highlights the critical role of the vz gate and its interplay with the open-system dynamics of quantum processors. We have demonstrated that a symmetric compilation of quantum gates with respect to the vz gate, e.g., the Y and $\overline{X}$ gates, significantly improves the fidelity of these gates. In particular, it removes an undesired asymmetry between states in the x-y plane of the Bloch sphere that is present when an asymmetric gate compilation is used instead. We have experimentally validated the advantage offered by a symmetric gate compilation using our in-house processor MUNINN as well as using the IBM cloud processor IBM_SHERBROOKE, showing in particular the impact on commonly used DD sequences, as well as on GHZ-state preservation.

Our findings highlight the need to carefully consider vz gate compilation in future studies, as well as the impact on previous studies that have used asymmetric gate compilations. Specifically, we have shown that asymmetric compilation can lead to unexpected outcomes, such as fidelity asymmetries and incorrect implementations of DD sequences. This can result in misleading interpretations

of earlier DD experiments. A case in point is that an asymmetric compilation of the Y gate has the effect that the standard XY4 DD sequence is actually an implementation of the UR_4 sequence, which does not suppress any undesired X-type interactions. In contrast, symmetric compilations preserve the intended gate operations and result in a faithful implementation of the desired DD sequences. A related direction for future research is the impact of our results on twirling-based experiments, e.g., in the context of probabilistic error cancellation [63,64], where we expect vz-gate-based compilations based on real Y gates to lead to more efficient suppression of off-diagonal terms in noise channels.

Going beyond DD and the Y gate, we have also demonstrated that symmetric compilation of arbitrary x-y–plane rotations can affect algorithmic performance using the example of GHZ-state preparation. In the Appendix, we further explore the effect on fidelity of random quantum circuits. Furthermore, we have explored the impact of pulse interference, which can introduce coherent errors even in DD sequences that are designed to be robust to such errors. We have demonstrated that these effects can be mitigated by intentionally increasing the pulse interval, highlighting the importance of optimizing the pulse interval for a given quantum processor. These results explain earlier observations where robust sequences have resulted in suboptimal performance; this effect can now be attributed to pulse-interference effects.

Future studies may focus on refining gate-compilation strategies and addressing pulse-interference effects to further enhance the fidelity of quantum gates.

ACKNOWLEDGMENT

This material is based upon work supported by, or in part by, the National Science Foundation Quantum Leap Big Idea under Grant No. OMA-1936388, by the Defense Advanced Research Projects Agency under Agreement HR00112230006, by the Intelligence Advanced Research Projects Activity (IARPA) under the Entangled Logical Qubits program through Cooperative Agreement Number W911NF23-2-0216, and by the U.S. Army Research Laboratory and the U.S. Army Research Office under contract/grant number W911NF2310255. The views, opinions and/or findings expressed are those of the author(s) and should not be interpreted as representing the official views or policies of the Department of Defense or the U.S. Government. In-house processor was fabricated and provided by the Superconducting Qubits at Lincoln Laboratory (SQUILL) Foundry at MIT Lincoln Laboratory, with funding from the Laboratory for Physical Sciences (LPS) Qubit Collaboratory. This research was conducted using IBM Quantum Systems provided through University of Southern California's IBM Quantum Innovation Center. The views expressed are those of the authors and do not reflect the official policy or position of IBM or the IBM Quantum team.

APPENDIX: SYMMETRIC COMPILATION IN RANDOM QUANTUM CIRCUITS

Arbitrary rotations are often used in quantum algorithms, such as random circuit sampling [65], variational quantum eigensolvers [66], quantum simulation [67], and the quantum Fourier transform [47]. In this appendix, we present various tests of the role of symmetric compilation in the setting of random quantum circuits.

We prepare five-qubit random circuits of depths 6–15 (the number of time steps). At each time step, we randomly assign single- or two-qubit gates to some of the qubits, arranged in a linear chain. Our experiments use the IBM_SHERBROOKE and IBM_MARRAKESH QPUs; the

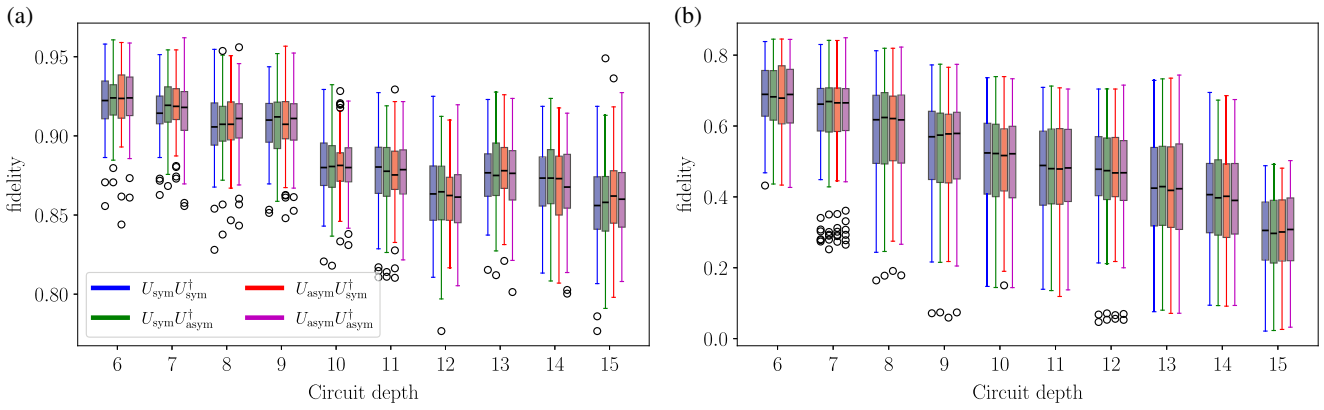

FIG. 8. A box plot of the fidelity of five-qubit random circuits of various circuit depths: (a) IBM_MARRAKESH; (b) IBM_SHERBROOKE. The red lines are medians, the boxes are the 25th–75th percentiles (quartiles), the whiskers are 1.5 times the interquartile range, and the circles denote outliers. At each circuit depth, we generate 100 random circuits distinguished only by the choice of symmetric or asymmetric compilation, as indicated by the legend. There is no statistically significant difference in fidelity between the four versions shown. The experiments reported in this plot have used temporally balanced circuits (ASAP for U and ALAP for $U^\dagger$) and bidirectional two-qubit gates.

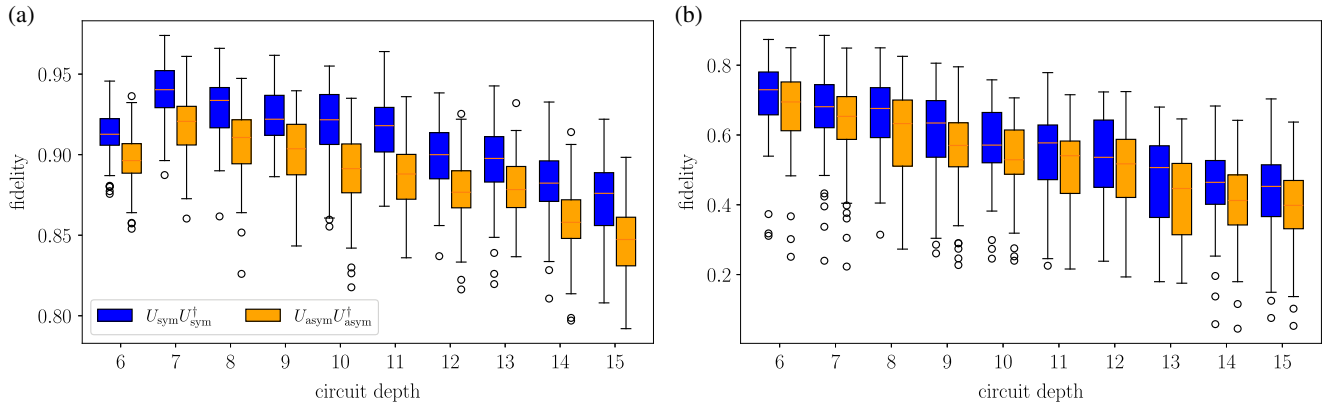

FIG. 9. A box plot of the fidelity of five-qubit random circuits of various circuit depths, without temporal balance (ASAP for both U and $U^{\dagger}$) and using only unidirectional two-qubit gates: (a) IBM_MARRAKESH; (b) IBM_SHERBROOKE. As in Fig. 8, the red lines are medians, the boxes are the 25th–75th percentiles (quartiles), the whiskers are 1.5 times the interquartile range, and the circles denote outliers. At each circuit depth we have 100 random circuits, each of which uses either all symmetric or all asymmetric compilation. The symmetric approach achieves consistently higher median and interquartile fidelities across all circuit depths.

former uses echo-cross-resonance [68] for its two-qubit gates, while the latter uses tunable couplers [69]. We randomly select two-qubit gates, including CNOT (controlled-NOT) and CZ (controlled-Z), from the following set: {CNOT, SWAP, CZ}, applying them only to adjacent qubits. This ensures that long-range two-qubit gates are not broken into more two-qubit gates on other qubits. We can choose to apply random two-qubit gates in one of two ways: either in a unidirectional manner, where they are always indexed as $q_i \rightarrow q_{i+1}$, or in a bidirectional manner, where they can be indexed as $q_i \leftrightarrow q_{i+1}$. Here, i represents the index of the qubits in our five-qubit linear chain.

Single-qubit gates are chosen uniformly from the set $\{X, H, R_\phi\}$, where H is the Hadamard gate and $R_\phi(\pi)$ is a rotation with a random angle ϕ such that $0 \leq \phi \leq 2\pi$. At least one of the five qubits always receives a gate at each time step, while the assignment of gates to the remaining four qubits is determined randomly. Thus, the total number of gates applied at each time step is dynamic and random. For each such random circuit U, we then run $U^{\dagger}$ and measure each qubit in the computational basis; the fidelity is computed as the fraction of all-zero bit strings. We generate 100 different random circuits for each circuit depth and run each random circuit once using the asymmetric choice of $R_\phi(\pi)$ [Eq. (17)] and once using the symmetric choice [Eq. (18)]. In QISKIT, the default scheduling options for a given circuit are either "as soon as possible" (ASAP) or "as late as possible" (ALAP) [54]. Due to the significant difference in duration between single- and two-qubit gates, either option alone for both U and $U^{\dagger}$ results in a temporal imbalance in the $UU^{\dagger}$ circuits. To ensure temporal symmetry across the entire circuit, we schedule U using ASAP and $U^{\dagger}$ using ALAP and then stitch the two circuits together. Finally, in order to demonstrate that the choice of compilation leads to different unitaries, we also perform the experiments $U_{\text{sym}}U_{\text{asym}}^{\dagger}$ and $U_{\text{asym}}U_{\text{sym}}^{\dagger}$. If the choice of compilation does not matter, then these experiments should be identical to $U_{\text{sym}}U_{\text{sym}}^{\dagger}$ and $U_{\text{asym}}U_{\text{asym}}^{\dagger}$.

In Fig. 8, we present our fidelity results for all four circuit types across both QPUs. For each circuit depth, the exact same circuit has been executed in the four different versions indicated: $U_{\text{sym}}U_{\text{sym}}^{\dagger}$, $U_{\text{sym}}U_{\text{asym}}^{\dagger}$, $U_{\text{asym}}U_{\text{sym}}^{\dagger}$, and $U_{\text{asym}}U_{\text{asym}}^{\dagger}$. The variations in fidelity across the four different circuit types are not statistically significant. This is the case when we use bidirectional gates as well as enforcing temporal balance using ASAP and ALAP.

In Fig. 9, we show the results of performing the same set of experiments but with unidirectional gates and without respecting temporal balance, i.e., using ASAP for both U and $U^{\dagger}$. In this case, we see that the $U_{\text{sym}}U_{\text{sym}}^{\dagger}$ circuits always yield a higher fidelity compared to $U_{\text{asym}}U_{\text{asym}}^{\dagger}$. We conjecture that this result might be due the fact that coherent errors build up and are not reversed in the temporally imbalanced case (while they are, to some extent, in the balanced case) and the symmetric compilation is more robust against such errors. However, this cannot be

TABLE I. A comparison of the random-circuit-sampling fidelity results based on temporal balance and two-qubit gate directionality. Fidelity results supporting the first and third rows are shown in Figs. 9 and 8, respectively. The results for the other two rows closely resemble Fig. 8 (not shown).

Temporal	Two-qubit gates	Fidelity
Imbalanced	Unidirectional	sym > asym
Imbalanced	Bidirectional	sym ≈ asym
Balanced	Bidirectional	sym ≈ asym
Balanced	Unidirectional	sym ≈ asym

the full explanation since, as shown in Table I, restoring bidirectionality also restores the performance parity between symmetric and asymmetric compilation, even in the temporally imbalanced case.

To explain why two-qubit gate directionality also plays a role, we conjecture that, since compiling two-qubit gates in terms of the native gate set will include asymmetric single-qubit gates, unidirectional two-qubit gates create a directional asymmetry that once again favors enforced symmetric single-qubit gates. A full explanation is left for future work.

[1] M. A. Nielsen and I. L. Chuang, *Quantum Computation and Quantum Information* (Cambridge University Press, Cambridge, United Kingdom, 2010).

[2] D. Lidar and T. Brun, Eds., *Quantum Error Correction* (Cambridge University Press, Cambridge, United Kingdom, 2013).

[3] D. Suter and G. A. Álvarez, Colloquium: Protecting quantum information against environmental noise, Rev. Mod. Phys. **88**, 041001 (2016).

[4] E. T. Campbell, B. M. Terhal, and C. Vuillot, Roads towards fault-tolerant universal quantum computation, Nature **549**, 172 EP (2017).

[5] Z. Cai, R. Babbush, S. C. Benjamin, S. Endo, W. J. Huggins, Y. Li, J. R. McClean, and T. E. O'Brien, Quantum error mitigation, Rev. Mod. Phys. **95**, 045005 (2023).

[6] P. Mell and T. Grance, The NIST definition of cloud computing, Special Publication (NIST SP) (2011) [online]. Available at https://doi.org/10.6028/NIST.SP.800-145 (accessed June 29, 2024).

[7] IBM Quantum, https://quantum.ibm.com/.

[8] P. J. Karalekas, N. A. Tezak, E. C. Peterson, C. A. Ryan, M. P. da Silva, and R. S. Smith, A quantum-classical cloud platform optimized for variational hybrid algorithms, Quantum Sci. Technol. **5**, 024003 (2020).

[9] J. Wurtz, A. Bylinskii, B. Braverman, J. Amato-Grill, S. H. Cantu, F. Huber, A. Lukin, F. Liu, P. Weinberg, J. Long, S.-T. Wang, N. Gemelke, and A. Keesling, Aquila: Quera's 256-qubit neutral-atom quantum computer, arXiv:2306.11727 [quant-ph].

[10] S. Blinov, B. Wu, and C. Monroe, Comparison of cloud-based ion trap and superconducting quantum computer architectures, AVS Quantum Sci. **3**, 033801 (2021).

[11] D. C. McKay, C. J. Wood, S. Sheldon, J. M. Chow, and J. M. Gambetta, Efficient Z gates for quantum computing, Phys. Rev. A **96**, 022330 (2017).

[12] S. Lloyd, Almost any quantum logic gate is universal, Phys. Rev. Lett. **75**, 346 (1995).

[13] A. Barenco, C. H. Bennett, R. Cleve, D. P. DiVincenzo, N. Margolus, P. Shor, T. Sleator, J. A. Smolin, and H. Weinfurter, Elementary gates for quantum computation, Phys. Rev. A **52**, 3457 (1995).

[14] P. Liu, R. Wang, J.-N. Zhang, Y. Zhang, X. Cai, H. Xu, Z. Li, J. Han, X. Li, G. Xue, W. Liu, L. You, Y. Jin, and H. Yu, Performing SU(d) operations and rudimentary algorithms in a superconducting transmon qudit for $d = 3$ and $d = 4$, Phys. Rev. X **13**, 021028 (2023).

[15] A. Vezvaee, E. Takou, P. Hilaire, M. F. Doty, and S. E. Economou, Avoiding leakage and errors caused by unwanted transitions in lambda systems, PRX Quantum **4**, 030312 (2023).

[16] M. Gullans, M. Caranti, A. Mills, and J. Petta, Compressed gate characterization for quantum devices with time-correlated noise, PRX Quantum **5**, 010306 (2024).

[17] R. B.-S. Tsai, H. Silvério, and L. Henriet, Pulse-level scheduling of quantum circuits for neutral-atom devices, Phys. Rev. Appl. **18**, 064035 (2022).

[18] L. E. Fischer, D. Miller, F. Tacchino, P. K. Barkoutsos, D. J. Egger, and I. Tavernelli, Ancilla-free implementation of generalized measurements for qubits embedded in a qudit space, Phys. Rev. Res. **4**, 033027 (2022).

[19] A. Vezvaee, N. Earnest-Noble, and K. Najafi, Quantum simulation of Fermi-Hubbard model based on transmon qudit interaction, arXiv:2402.01243 [quant-ph].

[20] A. S. Kazmina *et al.*, Demonstration of a parity-time-symmetry-breaking phase transition using superconducting and trapped-ion qutrits, Phys. Rev. A **109**, 032619 (2024).

[21] L. Viola and S. Lloyd, Dynamical suppression of decoherence in two-state quantum systems, Phys. Rev. A **58**, 2733 (1998).

[22] L. Viola, E. Knill, andS. Lloyd, Dynamical decoupling of open quantum systems, Phys. Rev. Lett. **82**, 2417 (1999).

[23] P. Zanardi, Symmetrizing evolutions, Phys. Lett. A **258**, 77 (1999).

[24] L.-M. Duan and G.-C. Guo, Suppressing environmental noise in quantum computation through pulse control, Phys. Lett. A **261**, 139 (1999).

[25] D. Vitali and P. Tombesi, Using parity kicks for decoherence control, Phys. Rev. A **59**, 4178 (1999).

[26] L. Viola and E. Knill, Robust dynamical decoupling of quantum systems with bounded controls, Phys. Rev. Lett. **90**, 037901 (2003).

[27] L. Viola and E. Knill, Random decoupling schemes for quantum dynamical control and error suppression, Phys. Rev. Lett. **94**, 060502 (2005).

[28] K. Khodjasteh and D. A. Lidar, Fault-tolerant quantum dynamical decoupling, Phys. Rev. Lett. **95**, 180501 (2005).

[29] G. S. Uhrig, Keeping a quantum bit alive by optimized π-pulse sequences, Phys. Rev. Lett. **98**, 100504 (2007).

[30] A. M. Souza, G. A. Álvarez, and D. Suter, Robust dynamical decoupling for quantum computing and quantum memory, Phys. Rev. Lett. **106**, 240501 (2011).

[31] G. Quiroz and D. A. Lidar, Optimized dynamical decoupling via genetic algorithms, Phys. Rev. A **88**, 052306 (2013).

[32] G. T. Genov, D. Schraft, N. V. Vitanov, and T. Halfmann, Arbitrarily accurate pulse sequences for robust dynamical decoupling, Phys. Rev. Lett. **118**, 133202 (2017).

[33] B. Pokharel, N. Anand, B. Fortman, and D. A. Lidar, Demonstration of fidelity improvement using dynamical decoupling with superconducting qubits, Phys. Rev. Lett. **121**, 220502 (2018).

[34] N. Ezzell, B. Pokharel, L. Tewala, G. Quiroz, and D. A. Lidar, Dynamical decoupling for superconducting qubits: A performance survey, Phys. Rev. Appl. **20**, 064027 (2023).

[35] S. Gustavsson, O. Zwier, J. Bylander, F. Yan, F. Yoshihara, Y. Nakamura, T. P. Orlando, and W. D. Oliver, Improving quantum gate fidelities by using a qubit to

measure microwave pulse distortions, Phys. Rev. Lett. **110**, 040502 (2013).
[36] A. M. Souza, Process tomography of robust dynamical decoupling with superconducting qubits, Quantum Inf. Process. **20**, 237 (2021).
[37] V. Tripathi, H. Chen, M. Khezri, K.-W. Yip, E. Levenson-Falk, and D. A. Lidar, Suppression of crosstalk in superconducting qubits using dynamical decoupling, Phys. Rev. Appl. **18**, 024068 (2022).
[38] C. Tong, H. Zhang, and B. Pokharel, Empirical learning of dynamical decoupling on quantum processors, arXiv:2403.02294 [quant-ph].
[39] A. Seif, H. Liao, V. Tripathi, K. Krsulich, M. Malekakhlagh, M. Amico, P. Jurcevic, and A. Javadi-Abhari, in *2024 ACM/IEEE 51st Annual International Symposium on Computer Architecture (ISCA)* (Buenos Aires, Argentina, 2024), pp. 310–324.
[40] A. Rahman, D. J. Egger, and C. Arenz, Learning how to dynamically decouple by optimizing rotational gates, Phys. Rev. Appl. **22**, 054074 (2024).
[41] F. Arute *et al.*, Quantum supremacy using a programmable superconducting processor, Nature **574**, 505 (2019).
[42] P. Jurcevic *et al.*, Demonstration of quantum volume 64 on a superconducting quantum computing system, Quantum Sci. Technol. **6**, 025020 (2021).
[43] E. Bäumer, V. Tripathi, D. S. Wang, P. Rall, E. H. Chen, S. Majumder, A. Seif, and Z. K. Minev, Efficient long-range entanglement using dynamic circuits, PRX Quantum **5**, 030339 (2024).
[44] B. Pokharel and D. A. Lidar, Demonstration of algorithmic quantum speedup, Phys. Rev. Lett. **130**, 210602 (2023).
[45] B. Pokharel and D. Lidar, Better-than-classical Grover search via quantum error detection and suppression, npj Quantum Inf. **10**, 23 (2024).
[46] P. Singkanipa, V. Kasatkin, Z. Zhou, G. Quiroz, and D. A. Lidar, Demonstration of algorithmic quantum speedup for an abelian hidden subgroup problem, arXiv:2401.07934 [quant-ph].
[47] E. Bäumer, V. Tripathi, A. Seif, D. Lidar, and D. S. Wang, Quantum Fourier transform using dynamic circuits, Phys. Rev. Lett. **133**, 150602 (2024).
[48] C. Gaikwad, D. Kowsari, C. Brame, X. Song, H. Zhang, M. Esposito, A. Ranadive, G. Cappelli, N. Roch, E. M. Levenson-Falk, and K. W. Murch, Entanglement assisted probe of the non-Markovian to Markovian transition in open quantum system dynamics, Phys. Rev. Lett. **132**, 200401 (2024).
[49] S. Shanto, A. Kuo, C. Miyamoto, H. Zhang, V. Maurya, E. Vlachos, M. Hecht, C. W. Shum, and E. Levenson-Falk, SQuADDS: A validated design database and simulation workflow for superconducting qubit design, Quantum **8**, 1465 (2024).
[50] V. Tripathi, H. Chen, E. Levenson-Falk, and D. A. Lidar, Modeling low- and high-frequency noise in transmon qubits with resource-efficient measurement, PRX Quantum **5**, 010320 (2024).
[51] V. Tripathi, D. Kowsari, K. Saurav, H. Zhang, E. M. Levenson-Falk, and D. A. Lidar, Benchmarking quantum gates and circuits, Chem. Rev. (2025).
[52] H. K. Ng, D. A. Lidar, and J. Preskill, Combining dynamical decoupling with fault-tolerant quantum computation, Phys. Rev. A **84**, 012305 (2011).
[53] A. A. Maudsley, Modified Carr-Purcell-Meiboom-Gill sequence for NMR Fourier imaging applications, J. Magn. Reson. (1969) **69**, 488 (1986).
[54] A. Javadi-Abhari, M. Treinish, K. Krsulich, C. J. Wood, J. Lishman, J. Gacon, S. Martiel, P. D. Nation, L. S. Bishop, A. W. Cross, B. R. Johnson, and J. M. Gambetta, Quantum computing with QISKIT, arXiv:2405.08810 [quant-ph].
[55] Z. Zhou, R. Sitler, Y. Oda, K. Schultz, and G. Quiroz, Quantum crosstalk robust quantum control, Phys. Rev. Lett. **131**, 210802 (2023).
[56] B. Evert, Z. G. Izquierdo, J. Sud, H.-Y. Hu, S. Grabbe, E. G. Rieffel, M. J. Reagor, and Z. Wang, Syncopated dynamical decoupling for suppressing crosstalk in quantum circuits, arXiv:2403.07836 [quant-ph].
[57] A. F. Brown and D. A. Lidar, Efficient chromatic-number-based multi-qubit decoherence and crosstalk suppression, arXiv:2406.13901.
[58] K. Khodjasteh and D. A. Lidar, Performance of deterministic dynamical decoupling schemes: Concatenated and periodic pulse sequences, Phys. Rev. A **75**, 062310 (2007).
[59] J. A. Gross, E. Genois, D. M. Debroy, Y. Zhang, W. Mruczkiewicz, Z.-P. Cian, and Z. Jiang, Characterizing coherent errors using matrix-element amplification, npj Quantum Inf. **10**, 123 (2024).
[60] G. S. Uhrig and D. A. Lidar, Rigorous bounds for optimal dynamical decoupling, Phys. Rev. A **82**, 012301 (2010).
[61] X. Peng, D. Suter, and D. A. Lidar, High fidelity quantum memory via dynamical decoupling: Theory and experiment, J. Phys. B: At. Mol. Opt. Phys. **44**, 154003 (2011).
[62] W. Morong, K. S. Collins, A. De, E. Stavropoulos, T. You, and C. Monroe, Engineering dynamically decoupled quantum simulations with trapped ions, PRX Quantum **4**, 010334 (2023).
[63] E. van den Berg, Z. K. Minev, A. Kandala, and K. Temme, Probabilistic error cancellation with sparse Pauli-Lindblad models on noisy quantum processors, Nat. Phys. **19**, 1116 (2023).
[64] Y. Kim, A. Eddins, S. Anand, K. Wei, E. Berg, S. Rosenblatt, H. Nayfeh, Y. Wu, M. Zaletel, K. Temme, and A. Kandala, Evidence for the utility of quantum computing before fault tolerance, Nature **618**, 500 (2023).
[65] A. Zlokapa, B. Villalonga, S. Boixo, and D. A. Lidar, Boundaries of quantum supremacy via random circuit sampling, npj Quantum Inf. **9**, 36 (2023).
[66] M. Cerezo, A. Arrasmith, R. Babbush, S. C. Benjamin, S. Endo, K. Fujii, J. R. McClean, K. Mitarai, X. Yuan, L. Cincio, and P. J. Coles, Variational quantum algorithms, Nat. Rev. Phys. **3**, 625 (2021).
[67] B. Fauseweh, Quantum many-body simulations on digital quantum computers: State-of-the-art and future challenges, Nat. Commun. **15**, 2123 (2024).
[68] V. Tripathi, M. Khezri, and A. N. Korotkov, Operation and intrinsic error budget of a two-qubit cross-resonance gate, Phys. Rev. A **100**, 012301 (2019).
[69] J. Stehlik, D. M. Zajac, D. L. Underwood, T. Phung, J. Blair, S. Carnevale, D. Klaus, G. A. Keefe, A. Carniol, M. Kumph, M. Steffen, and O. E. Dial, Tunable coupling architecture for fixed-frequency transmon superconducting qubits, Phys. Rev. Lett. **127**, 080505 (2021).